Infrared Spectroscopy Measurements of Residual Stresses in Polypropylene Fibers

ERIK ANDREASSEN[1,*] and OLE JAN MYHRE[2]

[1]SINTEF, P.O. Box 124 Blindern, N-0314 Oslo, Norway; [2]Statoil, N-3960 Stathelle, Norway

SYNOPSIS

Average residual stresses in polypropylene fibers, produced in a full-scale short-spin line, are estimated from the shift of the IR absorption peak at 975 cm^{-1}. Linearly polarized incident IR radiation is used to separate between stress components parallel and perpendicular to the fiber axis. For all the fibers in this study, the axial stress component is larger than the average stress perpendicular to the fiber axis. Axial and perpendicular stresses are correlated with draw ratio and polydispersity index. For narrow molecular weight distributions ($M_w/M_n < 4$–5), the axial stress increases with increasing draw ratio. Average stress perpendicular to the fiber axis decreases with increasing draw ratio for all the molecular weight distributions in this study (M_w/M_n = 3–6). Measurements of residual stresses are consistent with other results characterizing molecular structure and mobility. An expression for estimating the stored deformation energy is discussed. © 1993 John Wiley & Sons, Inc.

INTRODUCTION

The properties of plastic products, produced by various processes, are affected by residual stresses. The development, distribution, and relaxation of residual stresses have been studied both theoretically and experimentally, especially in relation to injection molding.[1,2] The study of residual stresses is interesting from a fundamental point of view in order to obtain a detailed understanding of topics such as deformation mechanisms and the development of microstructure. These studies also have practical value, for instance, in predicting long-term mechanical properties.

The causes for residual stresses in fibers can roughly be divided into two groups: (1) applied tension and (2) inhomogeneous cooling. Frozen-in molecular strains in the spinning stage and plastic deformations in the drawing stage belong to the first group. Thermal stresses due to cross-sectional temperature gradients belong to the second. These two effects will interact. In the spinning stage, this will, for instance, produce radial variations of orientation, which depend on both thermal gradients and spin-line tension, although the latter is the dominant cause for axial stresses.

Raman and infrared spectroscopy (IRS) have been used in a number of studies of molecular stress distributions, usually in combination with tensile loading devices. Raman spectroscopy is considered to be the best of the two for this application, but IRS is more widespread and somewhat simpler to use. Polypropylene (PP) has been the subject of several IRS studies of this kind: Zhurkov and Korsukov[3] studied chain scission under mechanical stress. Wool and Statton[4] studied stress relaxation and creep. Vettegren and Novak[5] estimated the true stresses on atomic bonds.

However, stress-related work on polymeric *fibers* is limited. A number of papers are published on stress distributions in high-performance polyethylene (PE) fibers. The experimental methods used in these studies are Raman spectroscopy and wide-angle X-ray scattering (WAXS). Several studies have reported correlations between molecular orientation, spin-line stress, and tenacity for as-spun PP fibers. Some stress analysis calculations have been done for the spinning stage,[6–8] mostly with amorphous polymers. Predicted residual stresses are found to correlate with measured birefringence and

* To whom correspondence should be addressed.

Journal of Applied Polymer Science, Vol. 50, 1715–1721 (1993)
 CCC 0021-8995/93/101715-07

spin-line tension. The filament tension in the drawing stage has also been studied,[9,10] but residual stresses originating from this stage have not been considered explicitly.

The spectroscopic papers mentioned above have discussed the changes in the spectra when deforming the samples *in situ*. This paper reports some correlations between the frequency shift of the stress-sensitive IR absorption peak at 975 cm^{-1} and the processing conditions of the filaments. The frequency shift is known to be a linear function of the tensile stress applied to PP samples.[11] Such a linear relationship is also calculated for molecular models. The stress-sensitive peak at 975 cm^{-1} is usually assigned to both amorphous and crystalline phases, although some assign it to the amorphous phase only. This IR mode is also strongly dichroic, with a transition moment angle close to zero. Therefore, the cross-sectional and phase-average stress of chains, with orientation parallel and perpendicular to the fiber axis, can be estimated from the frequency shift of this peak, using linearly polarized incident IR radiation.

Table I Parameters for Molecular Weight Distribution (as Determined by GPC) and Processing Conditions with Associated Ranges Examined in This Study

M_w[a]	160,000–230,000
M_w/M_n	3.4–5.8
Extrusion rate	3.3–15.8 cm^3/s
Extrusion temperature	220–280°C
Take-up velocity[b]	0.2–0.8 m/s
Draw ratio	1.5–3.5
Drawing temperature	140–180°C
Annealing ratio[c]	2–7%
Annealing temperature	150–180°C
Line velocity[d]	0.7–1.2 m/s
Final fiber dimension[e]	4–11 dtex

[a] The melt flow indices were in the range 8–25.
[b] After the spinning stage.
[c] The difference between input and output velocity for the annealing stage, divided by input velocity.
[d] The velocity at which the final fibers emerge.
[e] 1 dtex = 0.1 g/km, i.e., assuming constant density, this is a measure of cross-sectional area, which is proportional to the ratio of extrusion rate to line velocity.

EXPERIMENTAL

Fibers were produced in a full-scale short-spin line, and a spinneret with 9000 holes was used. The line consists of three stages: spinning, cold drawing, and annealing. A reduced factorial design was employed for the variation of molecular weight characteristics and typical industrial processing parameters (cf. Table I). All the polymers in this study are homopolymers with isotacticity in the range 96–98%.

IR transmission spectra of single fibers were obtained with a Perkin-Elmer FTIR 1725X, fitted with a microscope unit and a gold wire-grid polarizer. The fibers were fastened between two strips of double-coated adhesive tape. The tension imposed by this fastening arrangement can be neglected. This was found by recording spectra of fibers with loads of 1.5 and 2.6 mN clamped to one of the ends. The fiber tension was clearly higher with these loads than in the original fastening arrangement. However, the spectra were not affected by these loads, when fibers were either loaded (original arrangement followed by loads of 1.5 and 2.6 mN) or unloaded. This was expected, since the highest tension produced was 6 MPa (4 dtex fiber loaded with F = 2.6 mN), while the stress sensitivity factor is in the range 4–6 cm^{-1}/GPa.[12,13]

Spectra of 10–15 fibers were obtained for each processing condition. The resolution was 1 cm^{-1}. To quantify frequency shifts less than 1 cm^{-1}, two procedures were tried: nonlinear peak fitting (Voigt peaks and a polynomial background) and cubic spline fitting. The peak positions estimated with these techniques were approximately the same. The latter method was selected, because it was simpler to implement as part of an automated data-handling procedure. The uncertainty in this method is estimated to be ± 0.1 cm^{-1}. The standard deviation of the peak measurements was in the range 0.1–0.2 cm^{-1}.

RESULTS AND DISCUSSION

General

Stress generally affects both the position and the profile of stress-sensitive peaks. Splitting of stress-sensitive Raman peaks, due to bimodal stress distributions, has, for instance, been reported for strained PE fibers.[14] For the samples considered here, the peak profile variations are small and will not be considered. The peak frequency corresponds to an average stress level. Observed peak frequencies are in the range 972–975 cm^{-1}. This interval is smaller than for some experiments involving *in situ* straining.

For all the fibers in this study, the peak frequency obtained with incident IR radiation linearly polar-

ized parallel to the fiber direction ($\nu_{||}$) is lower than the frequency obtained with perpendicular polarization ($\nu_{\perp}$). The frequency is known to decrease with increasing stress, and the stress component in the fiber direction was expected to be larger than the components perpendicular to the fiber direction. There is not a strict equivalence between the components of the (continuum mechanical) stress and the stresses estimated with parallel and perpendicular polarization. The radial and circumferential stress components (of which both are perpendicular to the fiber axis) will, for instance, also have some influence on the chains that contribute when the polarization is parallel to the fiber direction. When the orientation is uniaxial, the chains that contribute to $\nu_{\perp}$ are mainly unoriented and unstrained.

No significant correlation is found between annealing stage parameters and frequency shifts. The annealing stage can, of course, still have influence on the residual stresses. This could be checked by analyzing fibers before and after the annealing stage.

The morphology and the mechanical properties of these fibers are dominated by the (solid-state) draw ratio. Hermans–Stein orientation factors[15] have been calculated for the peaks at 998, 2723, and 975 cm^{-1}. The first two peaks are claimed to represent the crystalline and amorphous phases, respectively.[15,16] The calculated orientation factors for the crystalline and amorphous phases (f_c and f_a) are in the ranges 0.4–0.9 (f_c) and 0.2–0.5 (f_a). An intermediate range is obtained for the 975 cm^{-1} band. The dichroic ratios (the ratio of absorption with parallel polarization to absorption with perpendicular polarization) for this peak have values between 2 and 10. Frequency shifts as reported in this article could be a source for error when dichroic ratios are calculated by standard procedures.[17]

Polarization Parallel to the Fiber Direction

The peak frequency of the 975 cm^{-1} band, obtained with polarization parallel to the fiber direction, is highly correlated with the cross-sectional area of the fibers. WAXS results, on the other hand, do not reveal any correlations between the morphology and the diameter of the fibers per se. A closer look at the spectra (Fig. 1) reveals similar shifts for the 998 cm^{-1} band, while the 842 and 1168 cm^{-1} bands are independent of the cross-sectional area. According to the literature,[11–13] the stress-sensitivity factors of the latter two are equal or higher than that of the former. The slopes of the base lines in Figure 1 differ. This effect was observed for all the fibers. However,

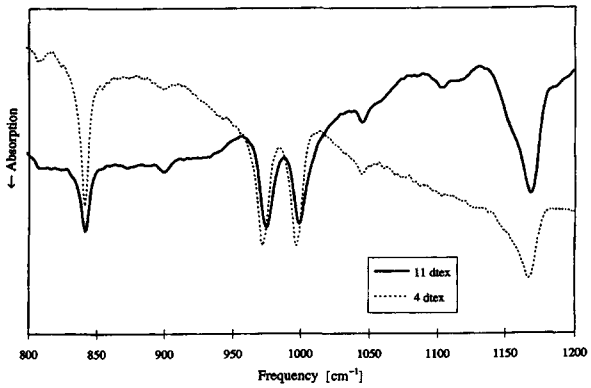

Figure 1 Typical spectra of 4 dtex and 11 dtex fibers using parallel polarization.

curve resolution, as described in the Experimental section, does not change the peak positions.

The fiber obtains its final diameter in the drawing oven. Hence, if the correlation between fiber diameter and $\nu_{||}$ is due to residual stress, this stress must originate from the drawing stage or the subsequent annealing stage. However, the most likely explanation of observed shifts and base lines is an optical effect. The diameter of the fiber is of the same order of magnitude as the wavelength of the IR radiation: 1000 cm^{-1} corresponds to 10 μm, and the diameter of a 4 dtex fiber is 24 μm.

Observed $\nu_{||}$ values are dominated by the diameter effect, but there is also some correlation with draw ratio, polydispersity index, melt flow index, and extrusion temperature. As expected, the former correlation is negative. The correlation with melt flow index and extrusion temperature is weak and will not be considered. The draw ratio dependence is observed only for narrow molecular weight distributions (cf. Table II and Fig. 2). For broad molecular weight distributions, it is remarkable that $\nu_{||}$ is not correlated with the draw ratio, which has such a large effect on crystalline and amorphous orientation factors. This implies that the molecular axial strain does not increase with increasing molecular orientation in this case. The number of chains oriented along the fiber axis increases with draw ratio, but the average stress in these oriented chains remains the same. The two normalized peak profiles obtained with parallel polarization in Figure 2 are almost equal, although the draw ratio is quite different for these two samples. The differences at the wings of these curves are due to the normalization procedure.

As mentioned in the preceding section, orientation factors and peak shifts have been obtained from the same spectra. The two fibers in Figure 2, which

Table II Selected Results for 4 dtex Fibers Illustrating the Effects of Draw Ratio and Polydispersity Index

PI[a]	MFI[b]	DR[c]	$\nu_{\parallel}$ (cm^{-1})	$\nu_{\perp}$ (cm^{-1})	$\Delta\nu$ (cm^{-1})
N	12	1.5	973.2	974.3	1.1
N	8	1.5	972.9	974.3	1.3
N	12	3.0	972.6	974.5	1.9
N	8	3.0	972.6	974.6	2.0
B	20	1.5	972.6	973.4	0.8
B	8	1.5	972.5	973.5	1.0
B	20	3.0	972.6	974.1	1.5
B	8	3.0	972.7	974.2	1.5

These eight fibers have different extrusion temperatures (220°C for #1, 5, and 8; 280°C for the rest). The draw-down ratios are also different (the inverse square of the fiber diameter is proportional to the product of draw ratio and draw-down ratio). However, the draw ratio is the dominant processing variable.

[a] Polydispersity index. N = "narrow," i.e., M_w/M_n = 3.3 – 3.6 B = "broad," i.e., M_w/M_n = 5.5 – 5.8.

[b] Melt flow index.

[c] Draw ratio.

have equal $\nu_{\parallel}$, have very different orientation factors: The fiber with draw ratio = 3.5 has f_c = 0.8 and f_a = 0.5, whereas the fiber with draw ratio = 1.5 has f_c = 0.5 and f_a = 0.3. However, these orientation factors are somewhat misleading: WAXS results reveal that fibers with draw ratio = 1.5 have bimodal crystallite orientation distributions, whereas fibers with draw ratio = 3.5 only have uniaxial orientation distributions, with preferred orientation of the crystallographic c-axis along the fiber axis. Therefore, the amount of oriented material in fibers with high and low draw ratio differs less than described by the orientation factors based on uniaxial orientation.

At high draw ratios, $\nu_{\parallel}$ is almost the same for narrow and broad molecular weight distributions (cf. Table II). At low draw ratios, the axial stress seems to be higher in fibers of broad molecular weight distributions. Similar trends are observed in measurements of crystallinity, molecular orientation, and tensile modulus; all these entities increase with increasing molecular weight distribution, especially when the draw ratio is low. These observations can be attributed to the fact that narrow and broad molecular weight distributions behave differently in the spinning stage as well as in the drawing stage.

In this study,[18] fibers of broad molecular weight distributions achieve higher levels of orientation and crystallinity in the spinning stage than do those of narrow distributions. This is probably due to the strain-induced crystallization, mainly caused by the high molecular weight tail.[19] Among the fibers with low draw ratios, these spinning stage effects dominate. (In the high take-up speed regime, which was not considered in this work, the highest orientation levels are reported for narrow molecular weight distributions.[20] This is probably due to different elongational viscosities vs. elongation rate for narrow and broad distributions.[21])

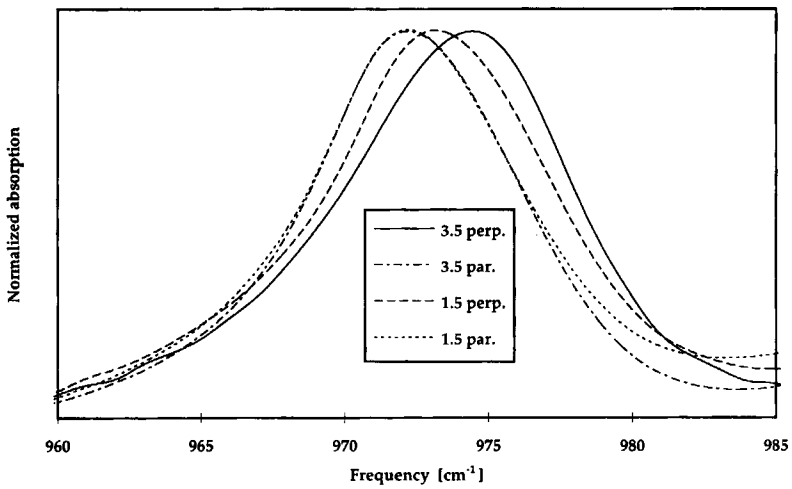

Figure 2 Normalized peaks obtained with parallel and perpendicular polarized incident IR radiation. Data for two fibers with the same diameter, but different draw ratios (1.5 and 3.5). This was accomplished by adjusting the take-up velocity for the spinning stage (which is the feed velocity for the drawing stage), i.e., the fibers were produced with the same extrusion rate and line speed. Each curve represents the average of 10–15 fibers. The material is a standard fiber grade with melt flow index = 14 and M_w/M_n = 5.5.

In the drawing stage, narrow distributions seem to experience a more homogeneous deformation,[22] which, in this case, leads to a higher average molecular orientation for a given draw ratio. Microvoids are also introduced in the drawing stage. Differential scanning calorimetry (DSC) and density measurements of the fibers in this study have revealed that the fraction of voids increases with increasing draw ratio.

VanderHart[23] observed that the concentration of mobile and oriented chains in noncrystalline regions of PE increases with decreasing drawing temperature and explains this by an increasing concentration of imperfections and voids. In this study, fibers of narrow and broad distributions have almost the same void fraction, crystallinity, and orientation at high draw ratios. At low draw ratios, fibers of broad distributions have a higher degree of crystallinity and orientation than that of fibers of narrow distributions, which are *paracrystalline* with an expected higher mobility. Hence, our estimates of axial residual stresses are consistent with other results characterizing molecular structure and mobility.

Polarization Perpendicular to the Fiber Direction

The peak frequency obtained with polarization perpendicular to the fiber direction ($\nu_\perp$) increases with increasing draw ratio and decreasing polydispersity index, as illustrated in Figure 2 and Table II. In contrast to the observations for $\nu_\parallel$, the draw ratio sensitivity of $\nu_\perp$ increases with increasing polydispersity index. For narrow molecular weight distributions, the draw ratio sensitivities of $\nu_\perp$ and $\nu_\parallel$ are almost the same, except for the sign. $\nu_\perp$ is also weakly correlated with melt flow index, draw-down ratio, fiber diameter, and extrusion temperature.

One explanation for the draw ratio dependence could be that as the draw ratio increases fewer chains contribute to $\nu_\perp$, and a larger fraction of the contributing chains might be "uncoupled" and unstrained. At high draw ratios, the "perpendicular" molecules are mainly in amorphous domains. Murthy et al.[24] characterized the amorphous phase in nylon 6 fibers by WAXS. They proposed that oriented amorphous chain segments are located in the interfibrillar regions, while unoriented segments, which are less likely to be strained, are located in the lamellar stacks within a fibril.

Both the radial and the circumferential stress components contribute to the average stress as measured by $\nu_\perp$. Kang and White[7] and Bell and Edie[8] calculated the radial distributions of the radial and circumferential stress components in as-spun amorphous fibers. The results in these two studies are qualitatively similar, except for opposite signs. For a crystalline anisotropic structure, the situation is more complex. Numerical simulation of stress development in crystallizable polymers is in an early stage. To the authors' knowledge, melt spinning has not yet been considered in simulations of this kind. However, such a simulation could be verified by comparisons with $\nu_\perp$ and $\nu_\parallel$. A reference frequency, corresponding to zero stress, and a stress-sensitivity factor are required for quantitative comparisons.

Stress Anisotropy

A quantitative comparison of stress anisotropy, involving fibers with different diameters, is difficult if the correlation between $\nu_\parallel$ and fiber diameter is due to an optical effect. No shifts in the 998 cm^{-1} band are observed for perpendicular polarization, and the frequency of this band is the same as for parallel polarization on 11 dtex fibers. If this is the "true" frequency, the frequency of the 975 cm^{-1} band represents the true axial stress in 11 dtex fibers, but not in 4 dtex fibers.

The difference between $\nu_\perp$ and $\nu_\parallel$ is plotted vs. draw ratio in Figure 3. The material is a standard grade with a relatively broad molecular weight distribution. Hence, the increase with increasing draw

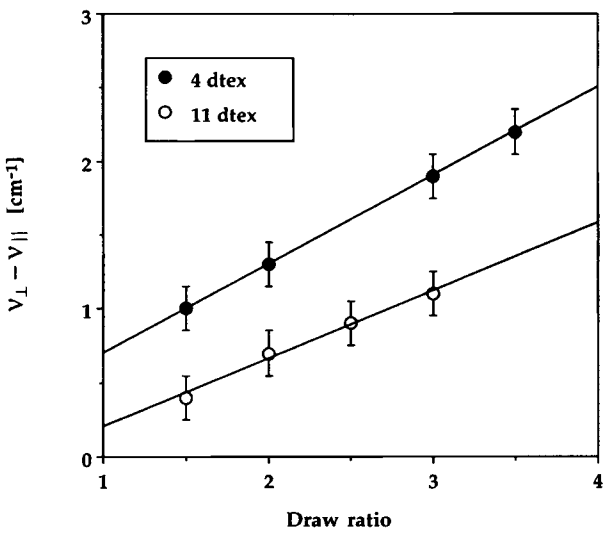

Figure 3 A measure of stress anisotropy vs. draw ratio. Fibers represented by the same symbol have the same diameter (cf. Fig. 2). The 4 dtex and 11 dtex series had the same filament velocity after the drawing stage. Obviously, due to the lower extrusion rate, the 4 dtex fibers have a higher "total" deformation ratio for a given draw ratio. The material is the same as in Figure 2.

ratio is due to $\nu_\perp$ and the separation between 4 dtex and 11 dtex fibers (which probably is due to an optical effect) is due to $\nu_\parallel$. This stress difference is a measure of stress anisotropy. As mentioned earlier, the fiber density decreases linearly on the same draw ratio interval, accompanied by a slight increase in the degree of crystallinity. This simultaneous increase in stress anisotropy and decrease in density might be coupled to the formation of fibrils and voids. If we compare observed stress anisotropies (using the stress-sensitivity factors cited in the Experimental section) with the stress–strain behavior of the fibers, the typical values of stress anisotropy corresponds to (applied) tensile stresses at elongations below 10%.

The stress-optical law, which is a linear relationship between differences in principal refractive indices (birefringence) and differences in principal stresses, is often used to estimate frozen-in stresses in amorphous polymers.[1] This approach is not valid for semicrystalline polymers. However, a plot of $\nu_\perp - \nu_\parallel$ vs. fiber birefringence (Fig. 4) shows a fairly linear relationship. The slight discrepancy (vertical shift) between the 4 dtex and 11 dtex fibers is another indication of the optical effects discussed earlier. Similar plots are obtained with the orientation factors mentioned above, instead of birefringence, as a measure of molecular orientation.

Stored Deformation Energy

The energy density due to frozen-in deformations can be estimated from spectroscopic data of this kind. A very simple model for this would be to assume a fraction f to be perfectly oriented, with average stress given by $\nu_\parallel$, while the remaining fraction $1 - f$ is unoriented and relaxed. This model is analog to the one used when interpreting IR dichroic ratios in terms of molecular orientation (see, e.g., Ref. 15). In this context, f is equivalent to the Hermans–Stein orientation factor. For small deformations in Hookean media, the elastic energy density, ϕ, can be written

$$\phi = \frac{\sigma^2}{2E} \tag{1}$$

where E is the tensile modulus, and σ, the stress (in general, both are matrices). With the simple model above, ϕ can be expressed as

$$\phi = Sf\beta^2(\nu_0 - \nu_\parallel)^2 \tag{2}$$

where ν_0 is a reference frequency, corresponding to zero stress (the stress level of the unoriented fraction, $1 - f$); S, an effective compliance; and β, the stress-sensitivity factor of the absorption peak. The nature of the compliance S is uncertain, due to the uncertainty in the phase assignment of the absorption peak.

The compliance decreases with increasing orientation, i.e., increasing f. The macroscopic modulus (inverse compliance) is approximately a linear function of f, but S also refers to molecular deformations. For small deformations, simple molecular theory yields a compliance that is inversely proportional to the square of the (molecular) draw ratio.[25] This draw ratio is again related to f obtained by IR dichroism.[15] Some limiting values for ϕ can be estimated, using the stress-sensitivity factors cited above. A maximum value is obtained with $S = 1/(2E_{min})$, $\nu_0 - \nu_\parallel = 3$ cm^{-1} (the range of observed peak positions, i.e., compression effects are neglected), and $f = 1$, where E_{min} is the minimum measured tensile modulus. This maximum ϕ is of the same order of magnitude as the measured heat of fusion. If the theoretical modulus of a perfect crystal is used, and minimum observed values are used for $\nu_0 - \nu_\parallel$ and f, the estimated ϕ will be 3–4 orders of magnitude smaller than the maximum value.

Equation (2) is a coarse simplification. Hearle[26] proposed that the deformation energy can be given by the sum of two terms. The first term is the energy of chain extension. This term can, for instance, be calculated using the inverse Langevin distribution function, and it represents the deformation of tie

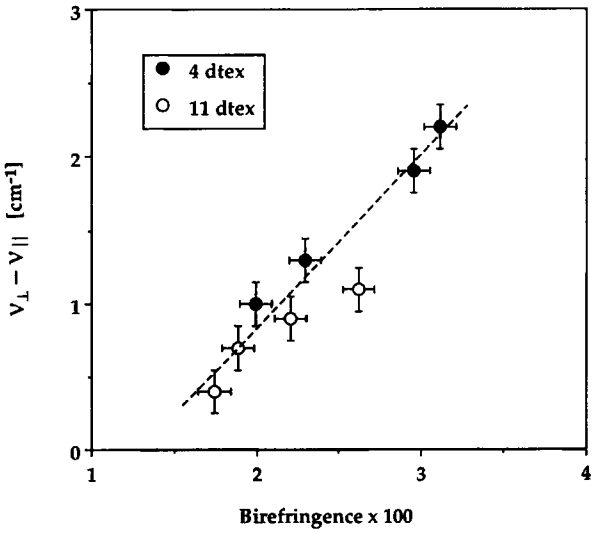

Figure 4 A measure of the difference in principal stresses vs. fiber birefringence. The fibers are the same as in Figure 3.

molecules. Hearle's second term, which he calls the energy of volume change, is similar to eq. (2).

Equation (2) is based on the average stress, and it is therefore probably not adequate for the analysis of mechanical failure. (Results from *in situ* straining, where the stress distribution have been obtained when the applied tensile stress is high, have been used for these purposes.) An area of possible application is the interpretation of DSC results obtained for oriented samples. Multiple melting peaks, observed for such samples, are claimed to be the combined effect of (endothermic) melting and (exothermic) shrinkage.[27]

Deformation calorimetry has been used in the literature[28,29] to measure the mechanical work and the heat of deformation during deformation. The difference between these two quantities is partly due to the buildup of internal stresses.[29] However, the deformation rates in calorimetry studies are lower than in this study, and the amount of stored energy depends on the deformation rate.[29]

The authors wish to thank M. D. Braathen and K. Grøstad at Statoil, and E. L. Hinrichsen at SINTEF, for helpful discussions. This paper is based on results from the "Expomat Fiber Project," supported by Statoil and the Royal Norwegian Council for Scientific and Industrial Research (NTNF).

REFERENCES

1. A. I. Isayev, in *Encyclopedia of Polymer Science and Engineering,* 2nd ed., Wiley, New York, 1989, Vol. 16, p. 747.
2. F. P. T. Baaijens, *Rheol. Acta,* **30,** 284 (1991).
3. S. N. Zhurkov and V. E. Korsukov, *J. Polym. Sci. Polym. Phys. Ed.,* **12,** 385 (1974).
4. R. P. Wool and W. O. Statton, *J. Polym. Sci. Polym. Phys. Ed.,* **12,** 1575 (1974).
5. V. I. Vettegren and I. I. Novak, *J. Polym. Sci. Polym. Phys. Ed.,* **11,** 2135 (1973).
6. H. H. George, *Polym. Eng. Sci.,* **22,** 292 (1982).
7. H. J. Kang and J. L. White, *Int. Polym. Process.,* **1,** 12 (1986).
8. W. P. Bell and D. D. Edie, *J. Appl. Polym. Sci.,* **33,** 1073 (1987).
9. A. Ziabicki, *Fundamentals of Fibre Formation,* Wiley, London, 1976.
10. B. D. Coleman and D. C. Newman, *J. Appl. Polym. Sci.,* **45,** 997 (1992).
11. R. P. Wool, *J. Polym. Sci. Polym. Phys. Ed.,* **13,** 1795 (1975).
12. Y.-L. Lee, R. S. Bretzlaff, and R. P. Wool, *J. Polym. Sci. Polym. Phys. Ed.,* **22,** 681 (1984).
13. K. Tashiro, S. Minami, G. Wu, and M. Kobayashi, *J. Polym. Sci. Polym. Phys. Ed.,* **30,** 1143 (1992).
14. J. A. H. M. Moonen, W. A. C. Roovers, R. J. Meier, and B. J. Kip, *J. Polym. Sci. Polym. Phys. Ed.,* **30,** 361 (1992).
15. R. J. Samuels, *Macromol. Chem. Suppl.,* **4,** 241 (1981).
16. F. M. Mirabella, Jr., *J. Polym. Sci. Polym. Phys. Ed.,* **25,** 591 (1987).
17. Y. Kobayashi, S. Okajima, and A. Narita, *J. Appl. Polym. Sci.,* **11,** 2515 (1967).
18. E. Andreassen and O. J. Myhre, to appear.
19. A. Peterlin, in *Flow-Induced Crystallization in Polymer Systems,* R. L. Miller, Ed., Gordon and Breach, New York, 1977.
20. F.-M. Lu and J. E. Spruiell, *J. Appl. Polym. Sci.,* **34,** 1521 (1987).
21. W. Minoshima, J. L. White, and J. E. Spruiell, *Polym. Eng. Sci.,* **20,** 1166 (1980).
22. P. Smith, P. J. Lemstra, and J. P. L. Pijpers, *J. Polym. Sci. Polym. Phys. Ed.,* **20,** 2229 (1982).
23. D. L. VanderHart, *Macromolecules,* **12,** 1232 (1979).
24. N. S. Murthy, S. T. Correale, and R. A. F. Moore, *J. Appl. Polym. Sci. Appl. Polym. Symp.,* **47,** 185 (1991).
25. L. H. Sperling, *Introduction to Physical Polymer Science,* Wiley, New York, 1986.
26. J. W. S. Hearle, *J. Appl. Polym. Sci. Appl. Polym. Symp.,* **47,** 1 (1991).
27. D. C. Sun and J. H. Magill, *Polym. Eng. Sci.,* **29,** 1503 (1989).
28. O. B. Salamatina, S. N. Rudnev, V. V. Voenniy, and E. F. Oleynik, *J. Thermal Anal.,* **38,** 1271 (1992).
29. Y. K. Godovsky, *Thermophysical Properties of Polymers,* Springer, Berlin, 1992.

Received September 14, 1992
Accepted May 4, 1993